



ALMA MATER STUDIORUM  
UNIVERSITÀ DI BOLOGNA

## ARCHIVIO ISTITUZIONALE DELLA RICERCA

### Alma Mater Studiorum Università di Bologna Archivio istituzionale della ricerca

From zero to infinity: Minimum to maximum diversity of the planet by spatio-parametric Rao's quadratic entropy

This is the final peer-reviewed author's accepted manuscript (postprint) of the following publication:

*Published Version:*

*Availability:*

This version is available at: <https://hdl.handle.net/11585/818815> since: 2021-04-15

*Published:*

DOI: <http://doi.org/10.1111/geb.13270>

*Terms of use:*

Some rights reserved. The terms and conditions for the reuse of this version of the manuscript are specified in the publishing policy. For all terms of use and more information see the publisher's website.

This item was downloaded from IRIS Università di Bologna (<https://cris.unibo.it/>).  
When citing, please refer to the published version.

(Article begins on next page)

This is the final peer-reviewed accepted manuscript of:

Rocchini, Duccio; Marcantonio, Matteo; Da Re, Daniele; Bacaro, Giovanni; Feoli, Enrico; Foody, Giles M.; Furrer, Reinhard; Harrigan, Ryan J.; Kleijn, David; Iannacito, Martina; Lenoir, Jonathan; Lin, Meixi; Malavasi, Marco; Marchetto, Elisa; Meyer, Rachel S.; Moudry, Vítězslav; Schneider, Fabian D.; Šímová, Petra; Thornhill, Andrew H.; Thouverai, Elisa; Vicario, Saverio; Wayne, Robert K.; Ricotta, Carlo: *From zero to infinity: Minimum to maximum diversity of the planet by spatio-parametric Rao's quadratic entropy*

GLOBAL ECOLOGY AND BIOGEOGRAPHY. Vol.30 ISSN 1466-822X

DOI: 10.1111/geb.13270

The final published version is available online at:

<https://dx.doi.org/10.1111/geb.13270>

Terms of use:

Some rights reserved. The terms and conditions for the reuse of this version of the manuscript are specified in the publishing policy. For all terms of use and more information see the publisher's website.

This item was downloaded from IRIS Università di Bologna (<https://cris.unibo.it/>)

**When citing, please refer to the published version.**

1 From zero to infinity: minimum to maximum diversity  
2 of the planet by spatio-parametric Rao's quadratic  
3 entropy

4  
5 November 8, 2020

6 **Abstract**

7 **Aim:** [The majority of work done to gather information on Earth diversity](#) has been  
8 carried out by in-situ data, with known issues related to epistemology (e.g., species  
9 determination and taxonomy), spatial uncertainty, logistics (time and costs), among  
10 others. [An alternative way to gather information about spatial ecosystem variability](#)  
11 [is the use of satellite remote sensing. It works as a powerful tool for attaining rapid](#)  
12 [and standardized information.](#) Several metrics used to calculate remotely sensed  
13 diversity of ecosystems are based on Shannon's Information Theory, namely on the  
14 differences in relative abundance of pixel reflectances in a certain area. Additional  
15 metrics like the Rao's quadratic entropy allow the use of spectral distance beside  
16 abundance, but they are point descriptors of diversity, namely they can account  
17 only for a part of the whole diversity continuum. The aim of this paper is thus to  
18 generalize the Rao's quadratic entropy by proposing its parameterization for the  
19 first time.

20 **Innovation:** The parametric Rao's quadratic entropy, coded in R, i) allows to  
21 represent the whole continuum of potential diversity indices in one formula, and ii)  
22 starting from the Rao's quadratic entropy, allows to explicitly make use of distances  
23 among pixel reflectance values, together with relative abundances.

24 **Main conclusions:** The proposed unifying measure is an integration between  
25 abundance- and distance-based algorithms to map the continuum of diversity given  
26 a satellite image at any spatial scale.

27 *Keywords:* biodiversity; ecological informatics; modelling; remote sensing; satellite  
28 imagery.

29

# 1 Introduction

Since Alexander von Humboldt (1769-1859), the spatial component of nature has played a relevant role in natural science. In the development of theoretical and empirical models in ecology, spatial structure represents a key concept to allow scientists to link ecological patterns to the generating processes and to the functional networking among organisms (Borcard and Legendre, 2002).

The majority of the work done to gather information about Earth diversity has been carried out by in-situ data, with known issues related to epistemology (e.g., species determination and taxonomy), spatial uncertainty, logistics (time and costs), among others (Rocchini et al., 2011).

Using satellite remote sensing can at least help attaining rapid and standardized information about Earth diversity (Gillespie, 2005; Rocchini et al., 2005). Furthermore, remote sensing can also be used to monitor some ecosystem functions and parameters such as temperatures, photosynthesis, vegetation biomass production and precipitation (Schimel et al., 2019; Zellweger et al., 2019) that can be useful to define the different niches of in-situ species, following first Goodall (1970) ideas, who envisaged future diversity measures as those based on niche theory (Hutchinson, 1959). The free access to remote sensing data (see Zellweger et al., 2019) has opened new ways to study ecosystem diversity and biodiversity issues (Rocchini et al., 2013). The spectral data related to pixels, as operational geographical units, are descriptions of pieces of land that allow us to define a new kind of Earth “diversity”, which may complement in-situ biodiversity measurement.

Diversity varies with area, thus investigating multiple spatial grains, until wide extents, is important to effectively monitor spatial diversity change in space and time (MacArthur et al., 1966). This is especially true in macroecology, where the primary aim

54 is to model large-scale spatial patterns to infer the ecological processes which generated  
55 them, particularly considering the recent effect of global changes worldwide (Hobohm et  
56 al., 2019). In order to determine the horizontal distribution of diversity within a satellite  
57 image (i.e. which areas within the image are more diverse than others), diversity indices  
58 are usually spatially referenced by calculating the index within a moving window.

59 Several metrics that measure diversity from satellites rely on the Shannon's theory of  
60 entropy (Shannon, 1948), with diversity being measured as  $H = -\sum_{i=1}^N p_i \log p_i$ , where  
61  $p_i$  is the proportion of the  $i$ -th pixel value (e.g., digital number, DN) found within a  
62 moving window containing  $N$  pixels. Shannon's  $H$  basically summarizes the partition of  
63 abundances (*sensu* Whittaker, 1965) by taking into account both relative abundance and  
64 richness of DNs (Figure 1).

65 However, Shannon's entropy is a point descriptor of (remotely sensed) diversity. As  
66 such, it shows only one part of the whole potential diversity spectrum at a glance. The  
67 use of generalized entropies has been advocated to face such problem. In this case, one  
68 single formula represents a parameterized version of a diversity index, thus providing a  
69 continuum of potential diversity indices. In the context of the measurement of diversity,  
70 the Rényi (1970) parametric entropy

$$H_\alpha = \frac{1}{1-\alpha} \log \sum_{i=1}^N p_i^\alpha \quad (1)$$

71

72 with  $0 \leq \alpha \leq \infty$  represents a powerful tool to account for the continuum of diversity  
73 (Figure 1).

74 One particularly convenient property of  $H_\alpha$  is that by varying the parameter  $\alpha$  there  
75 is a continuum of possible diversity measures, which differ in their sensitivity to rare and

76 abundant DNs, becoming increasingly dominated by the most common DNs for increasing  
77 values of  $\alpha$ . Note that for  $\alpha \rightarrow 1$ ,  $H_1$  equals the Shannon’s entropy. A similar formulation  
78 was then proposed by Hill (1973) who expressed parametric diversity as the “numbers  
79 equivalent” of Rényi generalized entropy. Appendix S1 provides the original formulation.

80 Rényi (and Hill) parametric functions summarize diversity by taking into account the  
81 pixel values of a satellite image and their relative abundances. However, they do not allow  
82 to explicitly consider the differences among these values. As an example, two arrays of  
83 9 pixels with maximum richness and evenness (i.e. both containing 9 different DNs with  
84 relative abundances  $p_i = \frac{1}{9}$ ) but differing in their values will attain the same Shannon  
85 diversity irrespective of the values of the DNs in both arrays.

86 By introducing a distance parameter  $d_{ij}$  among each pair of values  $i$  and  $j$ , Rao’s  
87 quadratic entropy (Rao, 1982)

$$Q = \sum_{i,j=1}^N p_i p_j d_{ij} \quad (2)$$

88

89 explicitly considers the differences among the pixel values in the calculation of diversity  
90 (Figure 1). Hence, two different pixels with values [2,3] will attain a lower diversity with  
91 respect to two pixels with values [0,100]. For instance, to make an ecological parallel, this  
92 is somewhat similar to the phylogenetic distance between two species: the values [2,3]  
93 would be equivalent to two sister species closely related on the tree of life while [1,100]  
94 would be equivalent to two very distant species on the tree of life.

95 The aim of this paper is thus to propose, for the first time, a parameterization of  
96 Rao’s quadratic entropy in order to provide a generalized entropy which accounts for  
97 both relative abundances and distances among pixel values. The proposed approach is

98 now part of the rasterdiv R package, a package dedicated to diversity measures of  
99 spatial matrices, increasing its capability to discern among different diversity measures  
100 by a single formula.

## 101 2 Spatio-parametric Rao's quadratic entropy

102 Inter-pixel spectral distances are directly related to landscape heterogeneity and they  
103 are capable of describing species habitats, starting with a satellite image (Rocchini et al.,  
104 2005). A satellite image can be viewed as a matrix of numbers describing Earth reflectance  
105 in different dimensions stored as pixels. A sensor per each light wavelength records the  
106 reflectance of a certain object in that wavelength which are stored into numbers in a  
107 certain range (e.g., digital numbers in 8 bits, ranging from 0 to 255). In general, the  
108 higher the variability in the spectral space defined by the pixel reflectance values, the  
109 higher the diversity of the ecosystem under study.

110 Consider a window of  $N$  pixels moving across the whole image to calculate a diversity  
111 index. Let  $i$  and  $j$  be two pixels randomly chosen with repetition within the moving  
112 window. Let  $d_{ij}$  be a symmetric measure of the (multi)spectral distance between  $i$  and  $j$   
113 such that  $d_{ij} = d_{ji}$  and  $d_{ii} = 0$ . Rao's  $Q$  (Rao, 1982) is defined as:

$$Q = \sum_{i,j=1}^N p_i p_j d_{ij} = \sum_{i,j=1}^N \frac{1}{N} \times \frac{1}{N} d_{ij} \quad (3)$$

114

115 Therefore,  $Q$  measures the expected (i.e. mean) distance between two randomly  
116 chosen pixels and  $\frac{1}{N}$  is the probability to extract each pixel. Note that, unlike  $H_\alpha$  or  
117  $K_\alpha$  the calculation of Rao's quadratic entropy is not limited to single bands but can



118 be extended to multispectral systems of any dimension. For the connection between  
119 quadratic entropy and variance, see [Rocchini et al., 2019](#).

120 Two parametric versions of quadratic entropy have been proposed by [Ricotta and](#)  
121 [Szeidl \(2006\)](#) and [Leinster and Cobbold \(2012\)](#). These parametric formulas were aimed  
122 at reconciling Rao's  $Q$  with parametric entropies. However, they have only been rarely  
123 used in practice.

124 A more direct approach for developing a parametric version of quadratic entropy  
125 stems from the work of [Guiasu and Guiasu \(2011\)](#). Let  $\omega_{ij} = \frac{1}{N} \times \frac{1}{N}$  be the combined  
126 probability of selecting pixels  $i$  and  $j$  in this order. [Guiasu and Guiasu \(2011\)](#) noted that  
127 Rao's  $Q$  can be expressed as a linear function of the combined probabilities of all pairs  
128 of pixels:

$$Q = \sum_{i,j=1}^N \omega_{ij} d_{ij} = \sum_{i,j=1}^N \frac{1}{N} \times \frac{1}{N} d_{ij} = \sum_{i,j=1}^N \frac{1}{N^2} d_{ij} \quad (4)$$

129

130 In practice, Rao's  $Q$  is the arithmetic mean of the distances  $d_{ij}$  between all pairs of  
131 pixels  $i$  and  $j$ . Hence, in order to implement a parametric version of Rao's  $Q$ , it seems  
132 natural to substitute the arithmetic mean in Equation [4](#) with a generalized mean ([Hardy](#)  
133 [et al., 1952](#)):

$$Q_\alpha = \left( \sum_{i,j=1}^N \omega_{ij} d_{ij}^\alpha \right)^{\frac{1}{\alpha}} = \left( \sum_{i,j=1}^N \frac{1}{N^2} d_{ij}^\alpha \right)^{\frac{1}{\alpha}} \quad (5)$$

134

135 This operation connects  $Q_\alpha$  with other diversity metrics that are expressed as gener-  
136 alized means, such as Hill's ([Hill, 1973](#)) or Jost's ([Jost, 2006](#)) numbers (Appendix S1)

137 equivalents (see also [Leinster and Cobbold, 2012](#)).

138 The Rao's  $Q$ , viewed as an arithmetic mean, is one of all the possible means in its  
 139 generalized form  $Q_\alpha$ :

$$Q_\alpha = \begin{cases} \alpha \rightarrow 0, Q_0 = \sqrt[N^2]{\prod_{i,j=1}^N d_{ij}} & \text{geometric} \\ \alpha = 1, Q_1 = Q = \sum_{i,j=1}^N \frac{1}{N^2} d_{ij} & \text{arithmetic} \\ \alpha = 2, Q_2 = \sqrt{\sum_{i,j=1}^N \frac{1}{N^2} d_{ij}^2} & \text{quadratic} \\ \alpha = 3, Q_3 = \sqrt[3]{\sum_{i,j=1}^N \frac{1}{N^2} d_{ij}^3} & \text{cubic} \\ \alpha \rightarrow \infty, Q_{\alpha \rightarrow \infty} = \max d_{ij} & \text{max}_d \end{cases} \quad (6)$$

140

141 The mathematical proof that i) for  $\alpha \rightarrow 0$   $Q_0$  corresponds to the geometric mean,  
 142 and ii) for  $\alpha \rightarrow \infty$   $Q_\infty$  corresponds to the maximum distance between pixel values pairs  
 143 is provided in Appendix S1.

144 Each generalized mean always lies between the smallest and largest of its values.  
 145 Increasing the parameter  $\alpha$  will increase the weight of the highest values of  $d_{ij}$ , thus  
 146 providing a continuum of potential diversity indices ([Figure 1](#)).

### 147 3 The algorithm

Starting from a satellite image, a spatial moving window might be used to make the calculation on predefined extents of analysis. The grain (*sensu* [Dungan et al., 2002](#)) will be the resolution of the image while the extent of analysis will be the size of the moving

window (Figure 2). The calculation is based on a distance matrix of type:

$$M_d = \begin{pmatrix} d_{\lambda_1, \lambda_1} & d_{\lambda_1, \lambda_2} & d_{\lambda_1, \lambda_3} & \cdots & d_{\lambda_1, \lambda_n} \\ d_{\lambda_2, \lambda_1} & d_{\lambda_2, \lambda_2} & d_{\lambda_2, \lambda_3} & \cdots & d_{\lambda_2, \lambda_n} \\ d_{\lambda_3, \lambda_1} & d_{\lambda_3, \lambda_2} & d_{\lambda_3, \lambda_3} & \cdots & d_{\lambda_3, \lambda_n} \\ \vdots & \vdots & \vdots & \ddots & \vdots \\ d_{\lambda_n, \lambda_1} & d_{\lambda_n, \lambda_2} & d_{\lambda_n, \lambda_3} & \cdots & d_{\lambda_n, \lambda_n} \end{pmatrix} \quad (7)$$

148

149 among all the potential pairs of pixels inside the moving window. The diagonal terms  
 150 of the matrix (which equal zero) will have no effect for  $\alpha > 0$  (Equation 6), since they  
 151 would enter the  $\sum$  term. On the contrary, for  $\alpha \rightarrow 0$ , they would enter the  $\prod$  term by  
 152 nullifying  $Q_0$ .

153 We coded the proposed parameterization of Rao's quadratic entropy as an R function,  
 154 implementing the previously developed `rasterdiv` package (Marcantonio et al. (2020),  
 155 <https://CRAN.R-project.org/package=rasterdiv>). The calculation of different  $Q_\alpha$   
 156 by automatically changing the range of potential  $\alpha$  values is done by the function `paRao`,  
 157 as:

```
158 > paRao(x, alpha=c(0:4, Inf), method="classic", 1
159   dist_m="euclidean", window=9, na.tolerance=0.5, simplify=3,
160   np=8, cluster.type="SOCK", diag=TRUE) 3
```

161 where `x` is the input dataset which can be a `RasterLayer` or a matrix class object,  
 162 `alpha` is the  $\alpha$  parameter of Equation 5, which can be a single value or a vector of inte-  
 163 gers. In the example above,  $\alpha$  is a vector of integers ranging from 0 to 4, plus `Inf`, which  
 164 in the R language is a reserved word representing positive infinity ( $\alpha \rightarrow \infty$ ). The option

165 `method` decides if `paRao` is calculated with 1 single layer (`classic`) or with more than  
166 one layer (`multidimension`). With `method="multidimension"` then `x` must be a list of  
167 objects. `dist_m` is the type of distance considered in the calculation of the index, and can  
168 be set to any distance class implemented in the R package `proxy`, such as `"euclidean"`,  
169 `"canberra"` or `"manhattan"`. Moreover, `dist_m` can also be an user-defined matrix of  
170 distances. However, if `method` is set to `"classic"` (unidimensional `paRao`) all distance  
171 types reduce to the Euclidean distance. The argument `window` is the side length in cells  
172 of the moving window (in this case set to 9), whereas `na.tolerance` is the proportion  
173 (0-1) of NA's cell allowed in a moving window: if the proportion of NA's cells in a moving  
174 window exceeds `na.tolerance` then the value of the moving window central pixel will be  
175 NA. The option `simplify` allows to reduce the number of decimal places to ease the cal-  
176 culation by reducing the number of numerical categories, i.e., if `simplify=3` only the first  
177 three digits of data will be considered for the calculation of the index. `np` is the number  
178 of parallel processes used in the calculation. If `np>1` then the `doParallel` package will  
179 be called for parallel calculation, and `cluster.type` will indicate the type of cluster to be  
180 opened (default is `"SOCK"`, `"MPI"` and `"FORK"` are the alternatives). The `diag` argument  
181 refers to the diagonal term of Equation 7. It will have no effect on the function for  $\alpha > 0$ ,  
182 while it will nullify the value of  $Q_\alpha$  if set to `TRUE`, as previously explained in Equation 7.  
183

### 184 **3.1 Global test of the parametric Rao's Q variation over the** 185 **planet**

186 We applied the algorithm to a Copernicus Proba-V NDVI (Normalized Difference Vege-  
187 tation Index) long term average image (June 21st 1999-2017) at 5km grain, also provided

188 in the `rasterdiv` package as a free `Rasterlayer` dataset which can be loaded by the  
189 function `data()` (Figure 2). The parametric Rao algorithm can also be applied to mul-  
190 tispectral data; in such a case distances are calculated in the multisystem created by  
191 the values of the pixels in each axis/band. The moving window passing throughout the  
192 whole image will return  $M_{Q_\alpha}$  matrices/layers where  $\alpha$  is the value chosen in the R function  
193 `paRao`.

194 With  $\alpha \rightarrow 0$  the  $\Pi$  in Equation 6 leads to zeroes throughout the whole map (Figure  
195 3). Increasing  $\alpha$  will increase the weight of higher distances among different values until  
196 reaching the maximum distance value for  $\alpha \rightarrow \infty$ . In this case the maximum turnover is  
197 reached and areas with maximum  $\beta$ -diversity will be apparent. In this case, a multitem-  
198 poral set is used (long term average NDVI from June 21st 1999-2017). Hence, areas with  
199 the highest spatial and temporal turnover are enhanced, namely major mountain ridges.  
200 We expect that using single frame images would lead to the enhancement of the spatial  
201 component of diversity.

202 Since the whole process is based on distances in a spectral space between pairs of pixels  
203 in terms of their “spectral characters” or in the “spectral space”, it is important to notice  
204 some cornerstone aspects on the use of distances from satellite images, especially when  
205 comparing different images or the same image in different times. In satellite images, the  
206 measure of distances could be impacted by: ii) the use of different sensors with different  
207 radiometric resolutions, as an example an 8-bit ( $2^8 = 256$  values) with respect to a 16-bit  
208 ( $2^{16} = 65536$  values) image, or ii) the radiometric calibration which has been performed,  
209 e.g. with a non-linear transform. Therefore, care should be taken when making use  
210 of distances in remote sensing data, explicitly taking into account how the vector of  
211 proportions between pixels belonging to some defined classes (e.g., digital numbers, DN)

212 was obtained.

213 The complete code of the function can be directly seen in R by typing the `paRao`  
214 function name. Moreover, a complete R coding session, to perform the above described  
215 analysis is provided in Appendix S2.

## 216 **3.2 Local case study: the diversity of vegetation greenness and** 217 **the ecoregions of California**

218 A comparison between in-situ and remotely sensed diversity at worldwide scale might  
219 be difficult due to known biases in e.g. sampling effort, taxonomies, spatial uncertainty  
220 (Rocchini et al., 2017). Hence, we decided to calculate the Rao's Q index on a NDVI  
221 raster layer of California (USA) to be compared with data in the field on native plant  
222 species diversity provided in Thornhill et al. (2017) from Baldwin et al. (2017). We chose  
223 California as a case study due to its high ecological diversity as well as to the availability  
224 of plant species field-data for this region.

225 In practice, we aimed at visualizing and describing differences in both diversity and  
226 structure of vegetation for the state of California, USA. First, an NDVI raster layer  
227 was derived from Copernicus Sentinel-2 data (European Space Agency, reference period:  
228 January 2017 to July 2018) and processed through Google Earth Engine to filter out  
229 cloud cover, select the greenest pixel of the time series and resample at 100 m pixel  
230 resolution. Then, the `paRao` R function was used to derive Rao's Q index, considering  
231 both the original formulation of the Rao's Q ( $\alpha = 1$ , Equation 6) and the formulation  
232 with  $\alpha \rightarrow \infty$  maximizing  $\beta$ -diversity (Figure 3), with a moving window of 9x9 pixels.

233 A map of plant species richness was derived using the potential distribution range of  
234 5,222 native California vascular plants modelled by Thornhill et al. (2017). Moreover,

235 a vector map reporting the ecoregions of California (level III) was downloaded from the  
236 United States Environmental Protection Agency. In Figure 4, we showed NDVI, the Rao's  
237 Q indices with  $\alpha = 1$  and  $\alpha \rightarrow \infty$  and plant species richness, reporting the boundaries  
238 of the different ecoregions for California. This comparison revealed macro-ecological and  
239 bio-geographical patterns which can be better interpreted considering the information  
240 condensed in the Rao's Q index.

241 For example, the ecoregion "Coast range" (labelled with 1 in Figure 4) is composed  
242 by low mountains covered by highly productive, rain-drenched evergreen forests. As a  
243 result, this region showed very high NDVI values but a low Rao's Q index (low vegetation  
244 structural diversity) and low to medium plant species richness. The adjacent "Klamath  
245 Mountain" ecoregion (2) is instead characterized by highly dissected ridges, foothills,  
246 and valleys. This region still showed high NDVI values but higher Rao's values with  
247 respect to region 1, which resulted in a high plant species richness. The diverse flora of  
248 this region, a mosaic of both northern Californian and Pacific Northwestern conifers and  
249 hardwoods, is rich in endemic and relic species. A similar pattern, although caused by  
250 opposite factors, was recognizable for the "Central Valley" region of California (3), which  
251 is composed of flat, urbanized and intensively farmed plains. The extensive presence of  
252 irrigated crops intersected with urbanized areas caused medium to high NDVI values and  
253 a very high apparent structural diversity. However, the same factors caused a low native  
254 species richness, especially in the drier southern portion of the valley. Finally, very dry  
255 and warm broad basins and scattered mountains characterize the "Mohave and Sonora  
256 ranges" ecoregions (4) which showed very low NDVI and Rao's Q values (with scattered  
257 higher values associated with local topographical variability) and low native plant species  
258 richness.

259 Passing from the pure Rao's Q index ( $\alpha=1$ ) to its parameterization with  $\alpha \rightarrow \infty$   
260 helped to increase the discrimination among areas, due to the fact that when  $\alpha \rightarrow \infty$   
261 the Rao's Q corresponds to the maximum distance ( $\beta$ -diversity) among pixel values in a  
262 site. Very similar gradients of the spatial heterogeneity of California (including BIOMOD  
263 variables, NDVI, elevation) as well as environmental DNA (eDNA) data are found in [Lin](#)  
264 [et al. \(2020\)](#).

## 265 4 Discussion

266 In this paper, we provided a straightforward solution to: i) account for distances in an  
267 Information Theory based metric, and ii) provide a generalized formula in order to avoid  
268 point description and account for the continuum of diversity. Diversity can be represented  
269 by different dimensions ([Nakamura et al., 2020](#)). Considering one single metric to account  
270 for the whole continuum of diversity metrics might be a powerful [addition](#) to the main  
271 framework. On the contrary, fragmenting the concept of diversity when trying to capture  
272 single aspects of the whole spectrum could be counterproductive.

273 The proposed unifying measure succeeded to integrate abundance- and distance-based  
274 algorithms over a wide variety of diversity metrics. We demonstrated that such integra-  
275 tion is not only theoretical but also applicable to real spatial data, considering several  
276 dimensions of diversity at the same time. Being part of the [rasterdiv](#) R package, the  
277 proposed method is expected to ensure high robustness and reproducibility.

278 Remote sensing is obviously not a panacea for all the organismic based diversities like  
279 taxonomic-, functional-, genetic-diversity but it can represent an important exploratory  
280 tool to detect diversity hotspots and their changes in space and time at the ecosystem  
281 level. First of all, it measures heterogeneity of the environment with indirect links to



282 the biodiversity of both plant and animal taxa, but also with potential discrepancies  
283 with species diversity, as in the presented case study of the native plant species diversity  
284 of California. This said, depending on the complexity and the resolution at which the  
285 proposed parameterized Rao's  $Q$  is applied, it might allow finding new insights on the  
286 ecological processes acting in a certain ecosystem to shape its diversity. In this paper,  
287 the examples provided were based on a single NDVI layer since i) it is a valuable index  
288 of vegetation health and ii) it is freely available in the `rasterdiv` package to reproduce  
289 the code proposed in this paper. We are aware that NDVI has very limited capacity  
290 to track diversity in some habitats like dense forests, because it is saturated at dense  
291 vegetation. From this point of view, imaging spectroscopy offers higher information  
292 content, also enabling plant functional trait retrievals (Jetz et al., 2016; Schneider et al.,  
293 2019) as well as structural traits by LiDAR data (Schneider et al., 2020). The application  
294 of the proposed algorithm to future spaceborne imaging spectroscopy is promising. In  
295 other words, the algorithm has been thought to be used with multiple layers, like a  
296 whole multispectral image or the most meaningful Principal Components (Peres-Neto et  
297 al., 2005), or land use classes probabilities derived from fuzzy set theory (Rocchini and  
298 Ricotta, 2007; Feoli, 2018). This is even one of the major advantages of the Rao's  $Q$   
299 metric which allows considering both abundance and distance among pixel values, thus  
300 being applicable to any continuous raster layer, or to any matrix combination, even in a  
301 multiple spectral system.

302 Creating a unique "umbrella" under which all of the potential metrics of diversity can  
303 be used is highly beneficial for e.g. monitoring the variation in time of biological systems  
304 considering two major axes: i) the  $\alpha$  parameter in Equation 5 providing information  
305 about the type of diversity at time  $t_0$ , ii) the temporal dimension from time  $t_0$  to time  $t_n$

306 given the same  $\alpha$  parameter. For the future, exploring such temporal dimension would  
307 allow gathering information of ecosystem changes in different diversity types at a glance.

308 Moreover, generalized entropy allows us to characterize the dimensionality of diversity  
309 (*sensu* Stevens and Tello, 2014) of different habitats/ecosystems. Those areas with a  
310 higher diversity dimensionality, namely a higher variability into the diversity spectrum  
311 would need a generalized measure to be fully undertaken. On the contrary, ecosystems  
312 with a lower dimensionality would have a lower difference among the different diversity  
313 measures with a flat curve of the diversity spectrum (Nakamura et al., 2020).

314 From a functional point of view, when all indices of diversity are highly correlated to  
315 each other (low dimensionality), it is expected that the ecological processes underlying  
316 diversity are just a few. On the contrary, with a lower correlation among indices (higher  
317 dimensionality) there might be a higher number of axes of variation coming out from  
318 different processes shaping ecological heterogeneity in space (Stevens and Tello, 2014).

319 There might be the possibility that a completely random matrix produces a pattern  
320 of diversity (Type I error). On the other side, a structured matrix could produce a very  
321 low diversity pattern (Type II error, Gotelli (2000)). In both cases, the parametric Rao's  
322  $Q$  could allow to determine, thanks to the use of a continuum of diversities, i) why a  
323 diversity pattern is still produced even in case of a random matrix, and ii) why a certain  
324 landscape shows a very low diversity in a certain point of the whole diversity spectrum.  
325 With point descriptors of diversity such inference cannot be done since the investigation  
326 is limited to a small window of the entire diversity spectrum, by basically relying on a  
327 single final number. In other words, the commonly asked question about what is the  
328 index which best describes diversity has no certain answer (Gorelick, 2011). Hence, the  
329 use of a trend of diversities will lead to the comprehension of hidden parts of the whole

330 diversity dimensionality.

331 Furthermore, it is expected that the ecological processes shaping diversity should act  
332 at defined spatial scales (Borcard and Legendre, 2002). Hence, different diversity types of  
333 the whole dimensionality spectrum are expected to show scale dependent patterns, being  
334 apparent only at certain scales and not at some others. The use of a continuum allows  
335 measuring the different diversity types altogether in a single step. Changing the extent  
336 of analysis by different moving windows would then allow to encompass different spatial  
337 structures at different scales.

338 While geographic gradients of diversity over space are complex to catch in their very  
339 nature, biodiversity measurement has mainly relied in the past on few formulas which  
340 represented an hegemony (Stevens et al., 2013). In this paper, we demonstrated that  
341 diversity is actually multifaceted and should be necessarily approached through a gener-  
342 alized approach.

## 343 5 Conclusion

344 In order to unfold the dimensionality of diversity methods to directly account for several  
345 aspects of diversity at a time are needed. From this point of view, generalized entropy  
346 undoubtedly represents a powerful approach for mapping the diversity continuum.

347 Furthermore, it might be profitably used to plot multitemporal trends (see e.g. Dor-  
348 nelas et al., 2014) of diversity metrics and discover previously imperceptible differences  
349 when making use of single metrics (Figure 5).

350 Metrics grounded in Information Theory ensure to make use of relative abundance of  
351 pixel values given the same richness in the moving window of analysis. However, distance  
352 metrics allow to also account for the relative dispersion in the spectral space of the cloud

353 of pixels in a certain area (Laliberté et al., 2020). The proposed parameterization of the  
354 Rao's  $Q$  explicitly considers the dispersion of pixel values in a spectral space (and their  
355 relative abundance) by allowing catching the whole dimensionality of diversity.

## 356 6 Data availability

357 The code and the data used in this paper are based on completely Free and Open Source  
358 Software, and they are available at the CRAN repository of the R package `rasterdiv`:  
359 <https://CRAN.R-project.org/package=rasterdiv>.

## 360 References

- 361 Baldwin, B.G., Thornhill, A.H., Freyman, W.A., Ackerly, D.D., Kling, M.M., Morueta-  
362 Holme, N., Mishler, B.D. (2017). Species richness and endemism in the native flora of  
363 California. *American Journal of Botany*, 104: 1-15.
- 364 Borcard, D., Legendre, P. (2002). All-scale spatial analysis of ecological data by means  
365 of principal coordinates of neighbour matrices. *Ecological Modelling*, 153: 51-68.
- 366 Dornelas, M., Gotelli, N.J., McGill, B., Shimadzu, H., Moyes, F., Sievers, C., Magurran,  
367 A.E. (2014). Assemblage time series reveal biodiversity change but not systematic loss.  
368 *Science*, 344: 296-299.
- 369 Evans, M.R., Grimm, V., Johst, K., Knuuttila, T., de Langhe, R., Lessells, C.M., Merz,  
370 M., O'Malley, M.A., Orzack, S.H., Weisberg, M., Wilkinson, D.J., Wolkenhauer, O.,  
371 Benton, T.G. (2013). Do simple models lead to generality in ecology? *Trends in Ecology*  
372 *& Evolution*, 28: 578-583.

373 Ferrier, S., Manion, G., Elith, J., Richardson, K. (2007). Using generalized dissimilarity  
374 modelling to analyse and predict patterns of beta diversity in regional biodiversity  
375 assessment. *Diversity and Distributions*, 13: 252-264.

376 Dungan, J.L., Perry, J.N., Dale, M.R.T., Legendre, P., Citron-Pousty, S., Fortin, M.-J.,  
377 Jakomulska, A., Miriti, M. and Rosenberg, M.S. (2002). A balanced view of scale in  
378 spatial statistical analysis. *Ecography*, 25: 626-640.

379 Gillespie, T.W. (2005). Predicting woody-plant species richness in tropical dry forests: a  
380 case study from South Florida, USA. *Ecological Applications*, 15: 27-37.

381 Gorelick, R. (2011). Do we have a consistent terminology for species diversity? The  
382 fallacy of true diversity. *Oecologia*, 167: 885-888.

383 Null model analysis of species co-occurrence patterns. *Ecology*, 81: 2606-2621.

384 Goodall, D.W. (1970). Statistical ecology, p. 99-124. In Johnston, R.F., ed. Annual review  
385 of ecology and systematics, Vol. 1. Annual Reviews, Palo Alto, California, USA.

386 Guiasu, R.C., Guiasu, S. (2011). The weighted quadratic index of biodiversity for pairs  
387 of species: a generalization of Rao's index. *Natural Science*, 3: 795-801.

388 Hardy, G., Littlewood, J.E., Polya, G. (1952). *Inequalities*. Cambridge University Press,  
389 Cambridge, UK.

390 Hill, M.O. (1973). Diversity and evenness: a unifying notation and its consequences.  
391 *Ecology*, 54: 427-431.

392 Hobohm, C., Janisova, M., Steinbauer, M., Landi, S., Field, R., Vanderplank, S.,  
393 Beierkuhnlein, C., Grytnes, J.-A., Vetaas, R.O., Fidelis, A., de Nascimento, L., Clark,

394 V.P., Fernandez-Palacios, J.M., Franklin, S., Guarino, R., Huang, J., Krestov, P., Ma,  
395 K., Onipchenko, V., Palmer, M.W., Fragomeni Simon, M., Stolz, C., Chiarucci, A.  
396 (2019). Global endemics-area relationships of vascular plants. *Perspectives in Ecology*  
397 *and Conservation*, 17: 41-49.

398 Hutchinson, G. 1959. Homage to Santa Rosalia or why are there so many kinds of animals?  
399 *American Naturalist*, 93: 145-159.

400 Feoli, E. (2018). Classification of plant communities and fuzzy diversity of vegetation  
401 systems. *Community Ecology*, 19: 186-198.

402 Jetz, W., Cavender-Bares, J., Pavlick, R., Schimel, D., Davis, F.W., Asner, G.P., Gu-  
403 ralnick, R., Kattge, J., Latimer, A.M., Moorcroft, P., Schaepman, M.E., Schildhauer,  
404 M.P., Schneider, F.D., Schrodte, F., Stahl, U., Ustin, S.L. (2016). Monitoring plant  
405 functional diversity from space. *Nature Plants*, 2: 16024.

406 Johnson, P.C.D., Barry, S.J.E., Ferguson, H.M., Müller, P. (2015). Power analysis for  
407 generalized linear mixed models in ecology and evolution. *Methods in Ecology and*  
408 *Evolution*, 6: 133-142.

409 Jost, L. (2006). Entropy and diversity. *Oikos*, 113: 363-375.

410 Laliberté, E., Schweiger, A.K., Legendre, P. (2019). Partitioning plant spectral diversity  
411 into alpha and beta components. *Ecology Letters*, 23: 370-380.

412 Leinster, T., Cobbold, C.A. (2012). Measuring diversity: the importance of species simi-  
413 larity. *Ecology*, 93: 477-489.

414 Leitão, P.J., Schwieder, M., Suess, S., Catry, I., Milton, E.J., Moreira, F., Osborne, P.E.,  
415 Pinto, M.J., van der Linden, S., Hostert, P. (2015), Mapping beta diversity from space:

416 Sparse Generalised Dissimilarity Modelling (SGDM) for analysing high-dimensional  
417 data. *Methods in Ecology and Evolution*, 6: 764-771.

418 Lin, M., Levi Simons, A., Curd, E.E., Harrigan, R.J., Schneider, F.D., Ruiz-Ramos,  
419 D.V., Gold, Z., Osborne, M.G., Shirazi, S., Schweizer, T.M., Moore, T.N., Fox, E.A.,  
420 Turba, R., Garcia-Vedrenne, A.E., Helman, S.K., Rutledge, K., Palacios Mejia, M.,  
421 Munguia Ramos, M.N., Wetzler, R., Pentcheff, D., McTavish, E.J., Dawson, M.N.,  
422 Shapiro, B., Wayne, R.K., Meyer, R.S. (2020). A biodiversity composition map of Cali-  
423 fornia derived from environmental DNA metabarcoding and Earth observation. *bioRxiv*  
424 2020.06.19.160374. doi: <https://doi.org/10.1101/2020.06.19.160374>

425 MacArthur, R.H., Recher, H., Cody, M. (1966). On the relation between habitat selection  
426 and species diversity. *American Naturalist*, 100: 319-327.

427 Marcantonio, M., Iannacito, M., Thouverai, E., Da Re, D., Tattoni, C., Bacaro, G.,  
428 Vicario, S., Rocchini, D. (2020). rasterdiv: Diversity Indices for Numerical Matrices.  
429 R package version 0.2-0. <https://CRAN.R-project.org/package=rasterdiv>

430 Nakamura, G., Gonçalves, L.O., Duarte, L.d.S. (2020). Revisiting the dimensionality of  
431 biological diversity. *Ecography*, 43: 539-548.

432 Patil, G.P., Taillie, C. (1982). Diversity as a concept and its measurement. *Journal of the*  
433 *American Statistical Association*, 77: 548-561.

434 Peres-Neto, P.R., Jackson, D.A., Somers, K.M. (2005). How many principal components?  
435 stopping rules for determining the number of non-trivial axes revisited. *Computational*  
436 *Statistics & Data Analysis*, 49: 974-997.

437 Rao, C.R. (1982). Diversity and dissimilarity coefficients: a unified approach. *Theoretical*  
438 *Population Biology*, 21: 24-43.

439 Rényi, A., 1970. *Probability Theory*. North Holland Publishing Company, Amsterdam.

440 Ricotta, C., Szeidl, L. (2006). Towards a unifying approach to diversity measures: bridg-  
441 ing the gap between the Shannon entropy and Rao's quadratic index. *Theoretical Pop-*  
442 *ulation Biology*, 70: 237-243.

443 Rocchini, D., Andreini Butini, S., Chiarucci, A. (2005). Maximizing plant species inven-  
444 tory efficiency by means of remotely sensed spectral distances. *Global Ecology and*  
445 *Biogeography*, 14: 431-437.

446 Rocchini, D., Delucchi, L., Bacaro, G., Cavallini, P., Feilhauer, H., Foody, G.M., He,  
447 K.S., Nagendra, H., Porta, C., Ricotta, C., Schmidtlein, S., Spano, L.D., Wegmann,  
448 M., Neteler, M. (2013). Calculating landscape diversity with information-theory based  
449 indices: A GRASS GIS solution. *Ecological Informatics*, 17: 82-93.

450 Rocchini, D., Garzon-Lopez, C.X., Marcantonio, M., Amici, V., Bacaro, G., Bastin, L.,  
451 Brummitt, N., Chiarucci, A., Foody, G.M., Hauffe, H.C., He, K.S., Ricotta, C., Rizzoli,  
452 A., Rosá, R. (2017). Anticipating species distributions: handling sampling effort bias  
453 under a Bayesian framework. *Science of the Total Environment*, 584-585, 282-290.

454 Rocchini, D., Hortal, J., Lengyel, S., Lobo, J.M., Jiménez-Valverde, A., Ricotta, C.,  
455 Bacaro, G., Chiarucci, A. (2011). Accounting for uncertainty when mapping species  
456 distributions: The need for maps of ignorance. *Progress in Physical Geography*, 35:  
457 211-226.

458 Rocchini, D., Luque, S., Pettorelli, N., Bastin, L., Doktor, D., Faedi, N., Feilhauer,



459 H., Féret, J.-B., Foody, G.M., Gavish, Y., Godinho, S., Kunin, W.E., Lausch, A.,  
460 Leitão, P.J., Marcantonio, M., Neteler, M., Ricotta, C., Schmidtlein, S., Vihervaara,  
461 P., Wegmann, M., Nagendra, H. (2018). Measuring  $\beta$ -diversity by remote sensing: a  
462 challenge for biodiversity monitoring. *Methods in Ecology and Evolution*, 9: 1787-1798.

463 Rocchini, D., Marcantonio, M., Da Re, D., Chirici, G., Galluzzi, M., Lenoir, J., Ricotta,  
464 C., Torresani, M., Ziv, G. (2019). Time-lapsing biodiversity: an open source method  
465 for measuring diversity changes by remote sensing. *Remote Sensing of Environment*,  
466 231: 111192.

467 Rocchini, D., Ricotta, C. (2007). Are landscapes as crisp as we may think? *Ecological*  
468 *Modelling*, 204: 535-539.

469 Schimel, D., Schneider, F.D., JPL Carbon and Ecosystem Participants (2019). Flux tow-  
470 ers in the sky: global ecology from space. *New Phytologist*, 224: 570-584.

471 Schneider, F.D., Ferraz, A., Schimel, D. (2019). Watching Earth's Interconnected Systems  
472 at Work. *Eos*, 100.

473 Schneider, F.D., Ferraz, A., Hancock, S., Duncanson, L.I., Dubayah, R.O., Pavlick, R.P.,  
474 Schimel, D.S. (2020). Towards mapping the diversity of canopy structure from space  
475 with GEDI. *Environmental Research Letters*, 15, 115006.

476 Shannon, C.E. (1948). A mathematical theory of communication. *Bell System Technical*  
477 *Journal*, 27: 379-423, 623-656.

478 Stevens, R.D., Tello, J.S. (2014). On the measurement of dimensionality of biodiversity.  
479 *Global Ecology and Biogeography*, 23: 1115-1125.

480 Stevens, R.D., Tello, J.S., Gavilanez, M.M. (2013). Stronger tests of mechanisms under-  
481 lying geographic gradients of biodiversity: insights from the dimensionality of biodi-  
482 versity. PLOS ONE, 8: e56853.

483 [Thornhill, A.H., Baldwin, B.G., Freyman, W.A., Nosratinia, S., Kling, M.M., Morueta-](#)  
484 [Holme, N., Madsen, T.P., Ackerly, D.D., Mishler, B.D. \(2017\). Spatial phylogenetics](#)  
485 [of the native California flora. BMC Biology 15: 96.](#)

486 Whittaker, R.H. (1965). Dominance and diversity in land plant communities. Science,  
487 147: 250-260.

488 Zellweger, F., De Frenne, P., Lenoir, J., Rocchini, D., Coomes, D. (2019). Advances in  
489 microclimate ecology arising from remote sensing. Trends in Ecology & Evolution, 34:  
490 327-341.

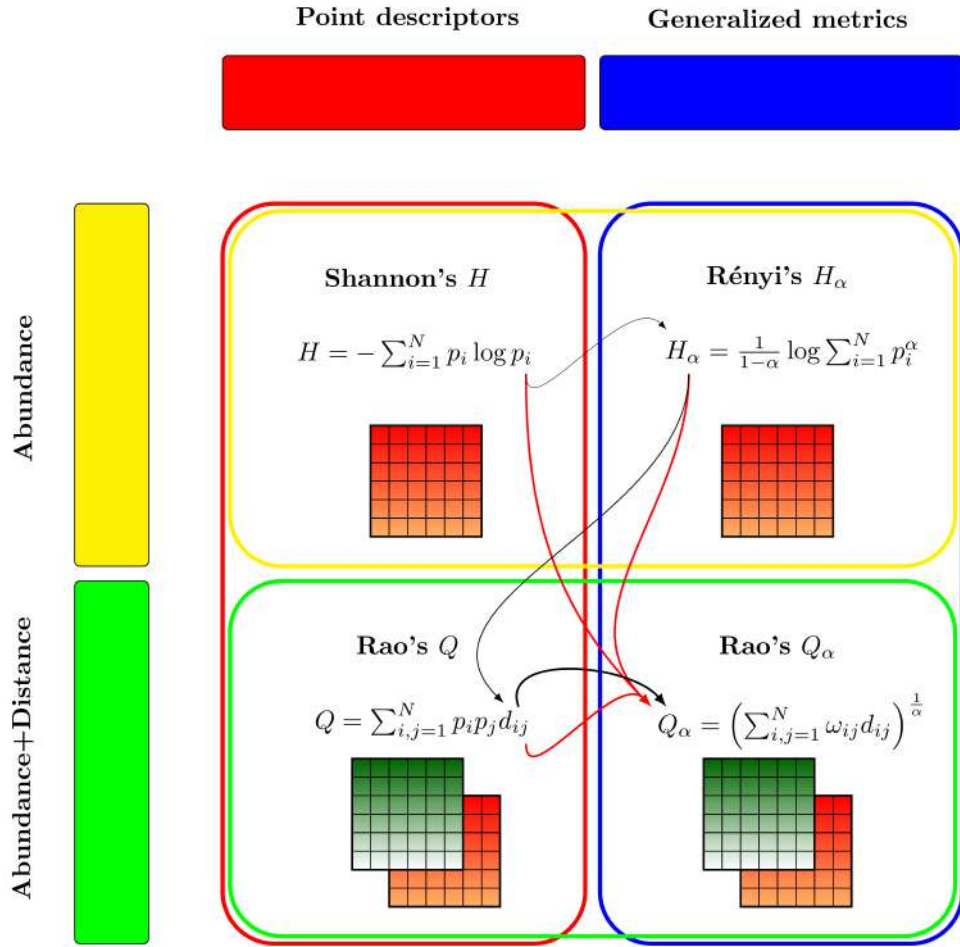


Figure 1: Grounding theory of this paper. Diversity measures can encompass abundance-based as well as abundance-distance-based metrics (yellow and green boxes, respectively). Abundance-distance-based metrics allow multiple layers to be used. The black lines represent the theoretical flow of this paper, with the thickness representing the complexity of each index, starting from Shannon’s Information Theory (point descriptor) to Rényi’s  $H_\alpha$  (generalized entropy), which do not make use of distance. Distance enters the Rao’s  $Q$  formula, but this is still a point descriptor of diversity. Finally, parametric Rao’s  $Q_\alpha$  comprises the use of distances and the generalized entropy concept. The red arrows represent the properties of the Rao’s  $Q_\alpha$ : i) it is grounded in Information Theory starting from Shannon’s  $H$ , ii) it is a generalized entropy like the Rényi  $H_\alpha$ , and iii) it makes use of distances like the Rao’s  $Q$ .

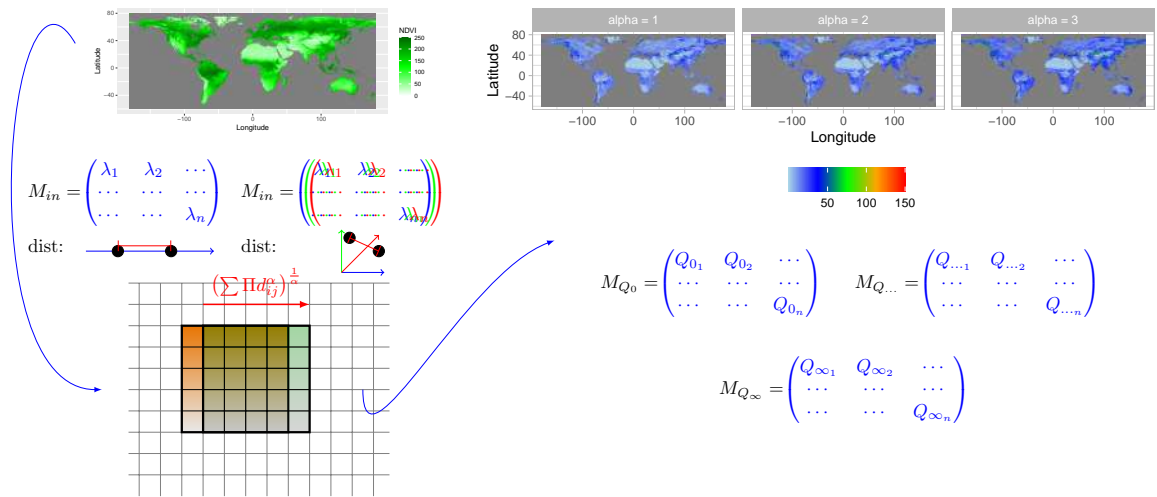


Figure 2: Starting from Copernicus Proba-V NDVI (Normalized Difference Vegetation Index) long term average image (June 21st 1999-2017) at 5km grain, parametric Rao's  $Q$  is calculated in a moving window. In this paper NDVI was used as a single layer to calculate distances on one axis, but several layers can be used as well. In this example, three layers (blue, green and red matrices) are shown to calculate distances. The algorithm is based on a moving window passing throughout the whole image, calculating the Rao's  $Q_{\alpha}$  and saving the output in the central pixel. In this example a moving window of 5x5 pixels is passing (red arrow) from one position (orange) to the other (green). The output is a stack of layers each of which represents a different mean of the whole generalized mean spectrum of Equation 5.

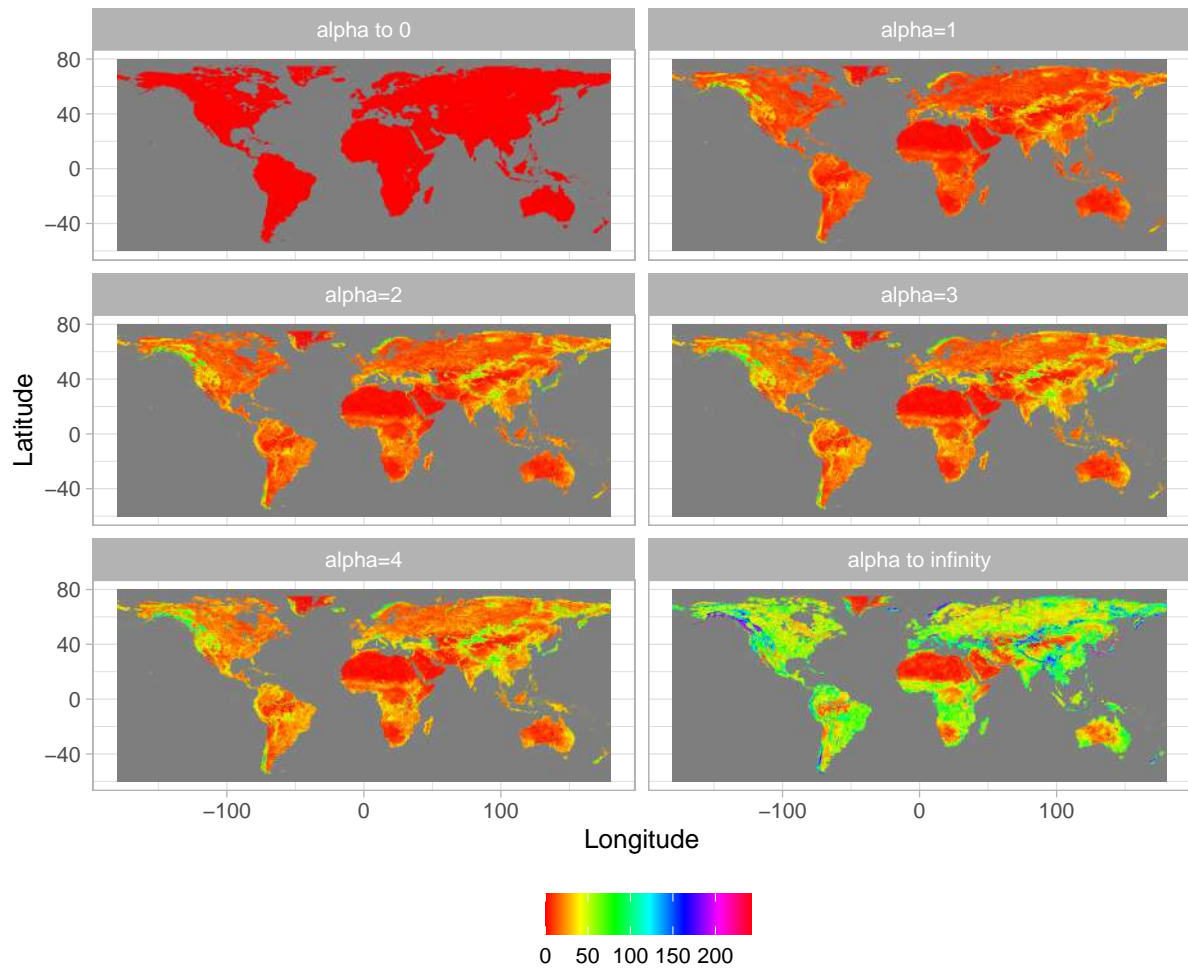


Figure 3: Output of the application of the algorithm shown in Figure 2, achieved by applying different  $\alpha$  values: from 0 to 4 until  $\alpha \rightarrow \infty$ . The higher the value of the parameter  $\alpha$ , the higher the weight of highest distances among pixel values, until reaching the maximum potential  $\beta$ -diversity (maximum distance) at  $\alpha \rightarrow \infty$ .

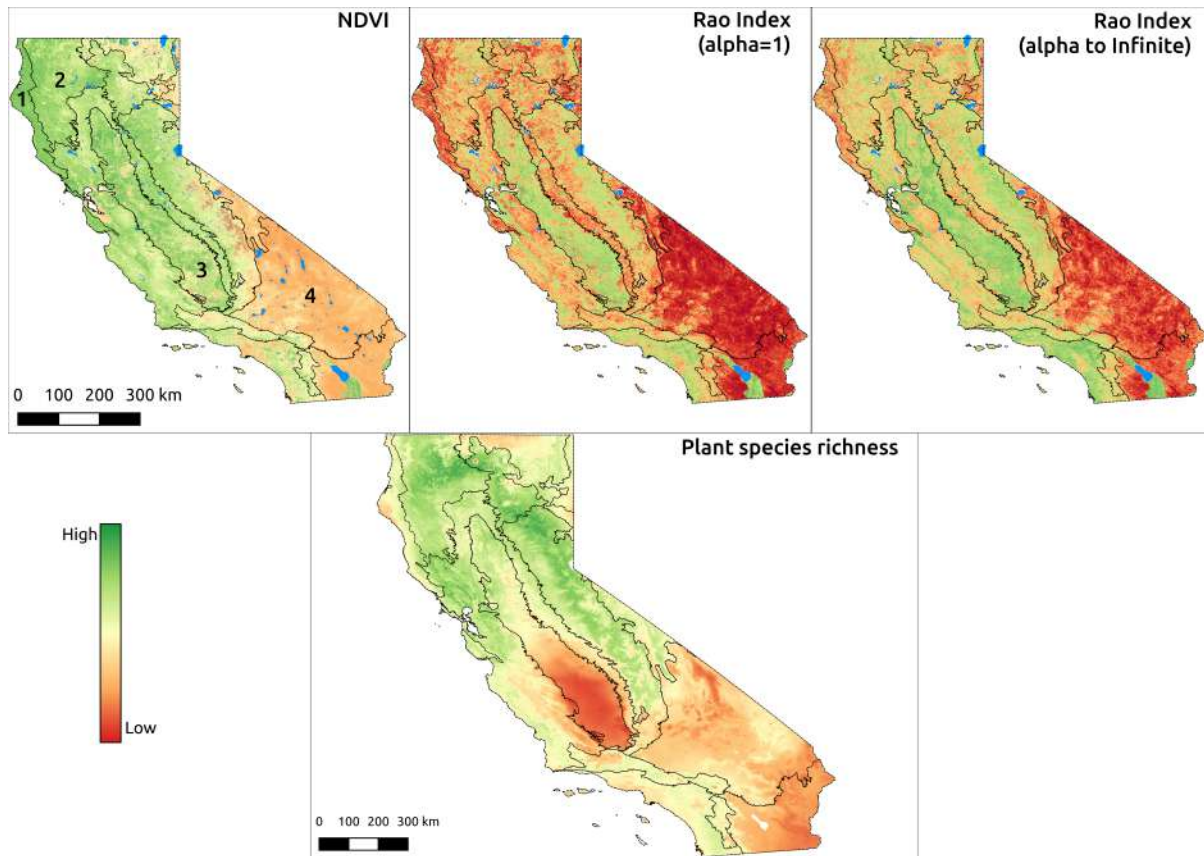


Figure 4: Comparison between NDVI, Rao's Q Index, native plant species richness for the ecoregions of California. The NDVI values shown in the top-left box (100 m resolution) were derived from the ESA Copernicus Sentinel-2 dataset then processed with Google Earth Engine and range between -0.26 (red) and 0.99 (green). The Rao's Q index shown in the top-right box was calculated from the NDVI map with  $\alpha=1$  and  $\alpha$  to infinite and a moving window of 9x9 pixels. High values are shown in dark green and represent pixel whose surrounding NDVI values are more "diverse" than pixel reported in red. The map reporting the potential native plant species richness of California (resolution: 810 m) was derived summing the binary potential distribution range of 5,222 native plant species modelled by [Thornhill et al. \(2017\)](#) and ranges between 134 (red) to 1029 (green) species per pixel (1 km<sup>2</sup>). The ecoregions considered in this paper are overlapped to the NDVI image: 1) Coast range (low mountains covered by highly productive, rain-drenched evergreen forests), 2) Klamath Mountain (highly dissected ridges, foothills, and valleys), 3) Central Valley (flat, urbanized and intensively farmed plains), 4) Mohave and Sonora ranges (very dry and warm broad basins).

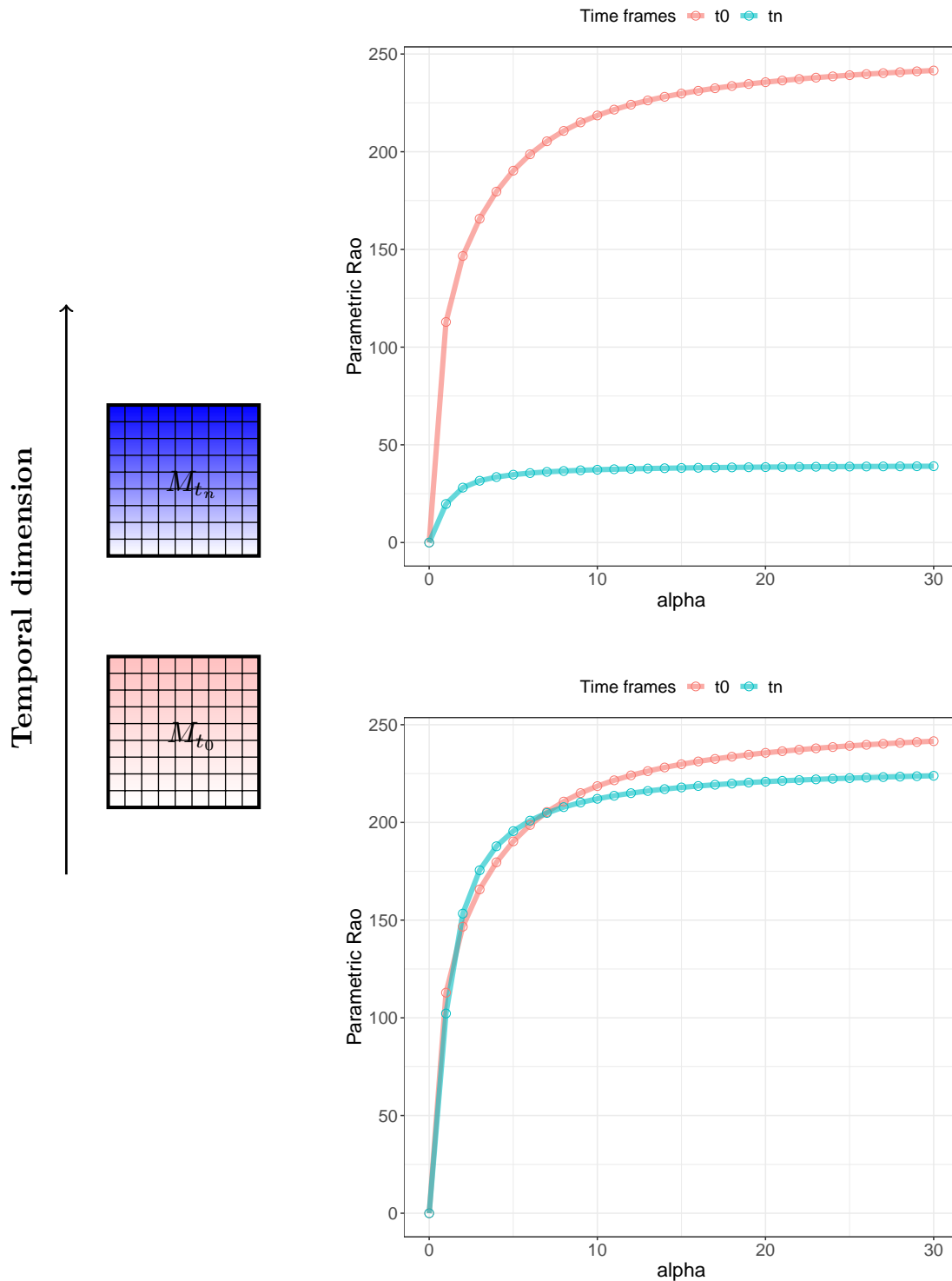


Figure 5: A theoretical example of the power of using generalized entropy for monitoring purposes. Given a landscape at times  $t_0$  (pink) and  $t_n$  (blue), calculating generalized entropy will allow the formation of a graph showing the continuum of Rao's  $Q$  values observed over a range of values for  $\alpha$ . The same landscape in different times might show an abrupt change (e.g., a catastrophic event) with an apparent diversity decrease (top). In this case, point descriptors (e.g., single  $\alpha$  values) of diversity may be sufficient to describe this pattern. When the change in diversity is subtle (bottom), using a point descriptor might fail to detect it but it becomes manifest in the continuum of diversities based on generalized entropy. The complete code for reproducing this theoretical example is available in Appendix S3.